GA–A21993

TRAVELING WAVE ANTENNA FOR FAST WAVE HEATING AND CURRENT DRIVE IN TOKAMAKS

by

H. IKEZI and D.A. PHELPS

JULY 1995

GENERAL ATOMICS

DISCLAIMER

DISCLAIMER

Portions of this document may be illegible in electronic image products. Images are produced from the best available original document.

GA–A21993

TRAVELING WAVE ANTENNA FOR FAST WAVE HEATING AND CURRENT DRIVE IN TOKAMAKS

by

H. IKEZI and D.A. PHELPS

This is a preprint of a paper submitted for publication in *Fusion Technology.*

Work supported by
U.S. Department of Energy
Contract DE–AC03–89ER51114

GENERAL ATOMICS PROJECT 3466
JULY 1995

Traveling Wave Antenna for Fast Wave Heating and Current Drive in Tokamaks*

H. IKEZI and D.A. PHELPS
General Atomics
San Diego, California 92186-9784, U.S.A.

Abstract

The traveling wave antenna for heating and current drive in the ion cyclotron range of frequencies is shown theoretically to have loading and wavenumber spectrum which are largely independent of plasma conditions. These characteristics have been demonstrated in low power experiments on the DIII–D tokamak, in which a standard four-strap antenna was converted to a traveling wave antenna through use of external coupling elements. The experiments indicate that the array maintains good impedance matching without dynamic tuning during abrupt changes in the plasma, such as during L– to H–mode transitions, edge localized mode activity, and disruptions. An analytic model was developed which exhibits the features observed in the experiments. Guidelines for the design of traveling wave antennas are derived from the validated model.

*This is a report of work sponsored by the U.S. Department of Energy under Contract No. DE-AC03-89ER51114.

Contents

Abstract iii
I. Introduction 1
II. Basic Properties of Traveling Wave Antenna 3
II.A. Inductor-Coupled Resonator Circuit 4
II.B. Mutual Inductance-Coupled Resonator Circuit 7
III. Experimental Setup 11
IV. Experimental Results 13
V. Comparison Between Experiments and Model 19
VI. Design Considerations 23
VII. Recirculation Circuit 25
VIII. Conclusions 31
IX. Acknowledgments 33
X. References 35

Figures

1. Schematic drawing of combline filter 3
2. Half-infinite circuit for experimentally tested, reduced impedance, and combline arrangements 5
3. Input impedance and real and imaginary part of propagation constant of circuit shown in Fig. 2(a) as a function of frequency 7
4. Input impedance and propagation constant of circuit shown in Fig. 2(c) as a function of frequency 8
5. Schematic diagram of the traveling wave antenna arrangement on the DIII–D tokamak 12
6. Transmission through the traveling wave antenna, reflection from input, and input-output phase delay as a function of frequency 14
7. Some plasma parameter signals of the tokamak plasma and time dependence of (reflected power)/(incident power) and (transmitted power)/(incident power) 15
8. Smith chart representation of input impedance 16
9. Transmission and reflection as a function of frequency 18

Figures (Continued)

10 Computed transmission, reflection, and Smith chart representation of input impedance 21
11. Computed reflection and attenuation as a function of antenna resistance 24
12. Schematic diagram of power recirculation 26
13. Fraction of radiated power, dumped power into dummy load, and reflected power back to transmitter, as a function of antenna resistance 28

I. Introduction

Fast waves in the ion cyclotron range of frequencies[1] have long been of interest for heating and current drive in tokamak plasmas. Fast wave antennas are typically arrays of two or four current-carrying straps placed on the outboard midplane of the plasma.[2,3] Antennas which radiate the fast wave into the plasma have two important requirements. First, effective coupling of the power must be made from the transmitter to the plasma. Second, for current drive, good spectral control must be maintained, since current drive is obtained by launching waves in one toroidal direction at a phase velocity which is comparable to the thermal speed of the electrons. Wave power is wasted if it is not radiated into the plasma at the correct phase velocity.

Optimum transfer of power to the plasma requires that the electrical impedance of the antenna strap, including the effects of the plasma, be matched to the impedance of the transmission line through an impedance matching network. In conventional antennas,[4] changes in the plasma conditions, such as a transition from L–mode to H–mode or the presence of edge localized mode (ELM) activity, cause large time-varying mismatches in the impedance. In many cases, readjustment of the impedance matching network must be performed on a millisecond time scale in order to prevent power reflected from the mismatch from affecting the power source. This rapid change in high power components is a severe technical challenge.[2,5,6]

Control of the toroidal wavenumber spectrum of the radiated power requires that more than two straps be arrayed in the toroidal direction. Fairly good toroidal directivity of the launched wave can be obtained with an antenna of four straps with phase delay between straps around 90 deg, but more straps are better. However, an impedance matching network with millisecond time response for each strap becomes a major problem of cost, space, control, and reliability.

The traveling wave antenna[7,8] offers distinct advantages over the conventionally fed antenna. The traveling wave antenna is a multiple element array with only two connections, the input and the output. Modeling presented here shows that good impedance matching and directivity can be maintained without dynamic tuning even during drastically changing plasma conditions. These results are verified through

experiments on the DIII–D tokamak, using a conventional four-strap antenna with external coupling elements. Extension of the modeling shows that a ten-element array or a four-element array with an external recirculating circuit can produce the desired highly directional wave spectrum and radiate more than 90% of the input power into changing plasma conditions without sacrificing impedance matching and array phasing.

II. Basic Properties of Traveling Wave Antenna

Moeller[7,8] proposed to use the combline filter structure as a fast wave antenna. The combline is a band-pass filter employed in the microwave frequency range.[9] It consists of an array of quarter-wavelength resonant straps which may be viewed as the radiating elements of the array antenna (see Fig. 1). The straps are inductively coupled to each other and form a slow traveling wave structure along the antenna in the direction perpendicular to the straps.

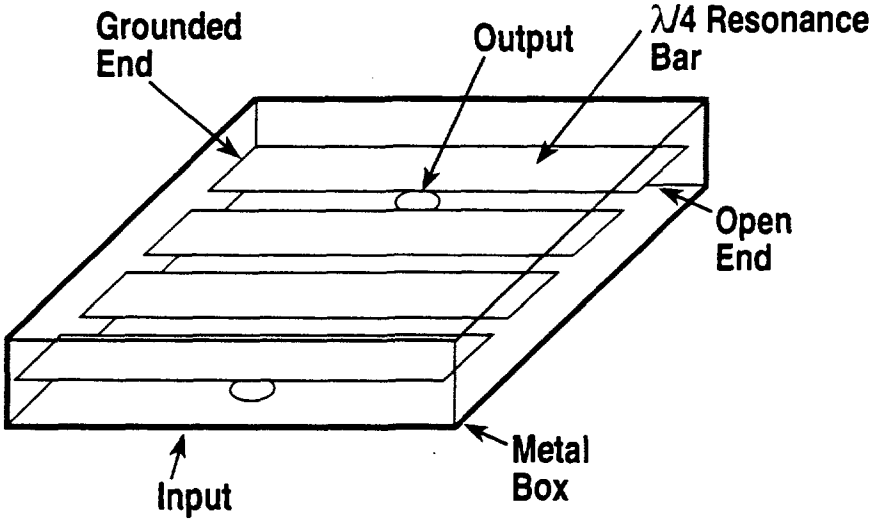

FIG. 1. Schematic drawing of combline filter.

If the combline is placed at the plasma boundary, the traveling combline field couples to the fast wave in the plasma. The coupling strength determines the wave damping rate along the combline. If the combline length is longer than the damping length, then all power fed to the combline is radiated into the plasma. The phase velocity is frequency-dependent and may be made equal to the electron speed in the plasma.

The input impedance of the combline is determined by the mutual inductance between the adjacent straps, which determines the wave energy transfer rate from one strap to the next strap. The radiation into the plasma, *i.e.*, the plasma loading, changes the impedance. However, the change is small if the mutual inductance is large, so that the wave energy on a strap is transferred to the next strap before radiating into the plasma significantly. *This is a very important property because it enables us to maintain good impedance matching without dynamic tuning when the plasma loading changes.* The larger mutual inductance, however, reduces the radiation power per strap meaning that larger numbers of straps are necessary to radiate all power before the wave reaches the end of the structure. These properties can be realized not only by the combline structure but also by any array of coupled resonators. A configuration we are interested in is shown in Fig. 2(a) which can be constructed from the antenna array existing in the DIII–D tokamak. The resonators consist of combinations of antenna straps and transmission lines and are coupled by inductors instead of mutual inductances between antenna elements.

The input impedance and the complex wavenumber of a half-infinitely long coupled resonator system may be calculated easily to provide a useful guideline for understanding the properties of the traveling wave antenna. We will show two cases (i) the infinitely long version of the experimentally tested antenna shown in Fig. 2(a) and (b), and (ii) the lumped circuit model of the original combline antenna shown in Fig. 2(c).

II.A. Inductor-Coupled Resonator Circuit

In Fig. 2(a) the antenna straps are modeled by a series connection of the inductance L_a and the resistance R_a. The resistance includes both the ohmic resistance of the strap and the radiation resistance. Consider the propagating voltage and current signals at the midpoint of the coupling inductor, given by

$$\left.\begin{aligned} V(n) &= V_0 \exp(i\omega t - iKn) \\ I(n) &= I_0 \exp(i\omega t - iKn) \end{aligned}\right\} . \tag{1}$$

Here, n is the number of resonator elements counting from the input. A simple calculation gives the input impedance Z and the wavenumber K

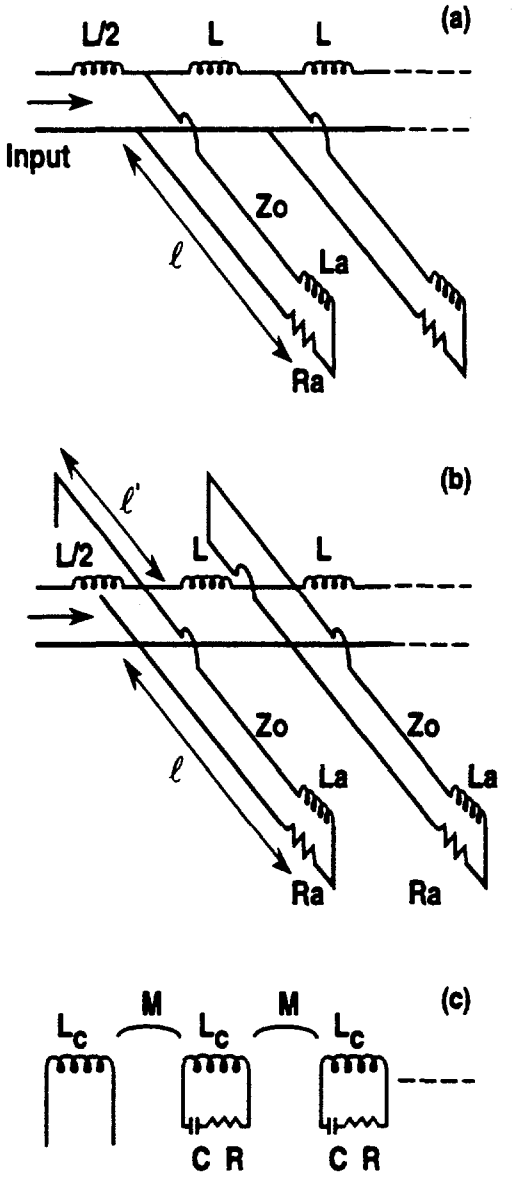

FIG. 2. Half-infinite circuit for (a) the experimentally tested arrangement, (b) the reduced impedance arrangement, and (c) the combline arrangement.

$$\left.\begin{aligned} Z &= V_0/I_0 = \left(Z_1 Z_2 + Z_1^2/4\right)^{1/2} \\ \sin^2(K/2) &= -\,Z_1/4\,Z_2 \end{aligned}\right\}\,, \tag{2}$$

where

$$\left.\begin{aligned} Z_1 &= i\omega L/2 \\ Z_2 &= Z_0 \frac{(Z_a/Z_0+1)+(Z_a/Z_0-1)\,e^{-2ik\ell}}{(Z_a/Z_0+1)-(Z_a/Z_0-1)\,e^{-2ik\ell}} \\ Z_a &= R_a + i\omega L_a \quad , \qquad k=\omega/u \\ \omega_0 &= \pi u/2\ell \end{aligned}\right\} \quad . \tag{3}$$

Z_a is the strap impedance, Z_0 is the vacuum feedthrough impedance, k is the wave-number in the feedthrough transmission line which has a length of ℓ, and the signals propagate with the speed of u in this transmission line. We employ the frequency ω_0, at which the quarter-wavelength equals ℓ, as a unit of frequency.

An example of Z and K as a function of frequency is shown in Fig. 3. The passband is the frequency range $1 \lesssim \omega/\omega_0 \lesssim 1.2$ in this case. The following are the general properties of the circuit.

(i) The passband width increases as the coupling inductance L is reduced. This property enables us to control the bandwidth easily.

(ii) The real part of the impedance Z_r is much larger than the imaginary part Z_i in the passband. The imaginary part is always inductive. Z_r is largest at the lowest end of the passband and monotonically decreases to $Z_r/Z_0 \simeq 1$ at the upper end. Z_r at the lowest end of the band decreases as R_a/Z_0 is increased, but the midband value does not depend much on R_a/Z_0 [compare two curves for different R_a/Z_0 in Fig. 3(a)]. *This insensitivity to R_a/Z_0 gives rise to the very important feature that changes in plasma loading do not affect the impedance much.* The high impedance $Z_r \gg Z_0$ of this circuit may be reduced to $Z_r \simeq Z_0$ by adding shorted end transmission line as shown in Fig. 2(b). The lower impedance version is preferable at the higher power operations and is analyzed later in this paper.

(iii) The imaginary part of K, which is the damping rate K_i, is small in the passband (by definition). K_i at the midband increases as the loading R_a/Z_0 is increased. K_i is inversely proportional to the bandwidth. The real part K_r is nearly zero at the lowest end of the passband, *i.e.*, the currents in all antenna straps are in-phase. K_r increases to nearly π at the upper end of the passband, *i.e.*, the currents in the nearest neighbor straps are out-of-phase. The frequency

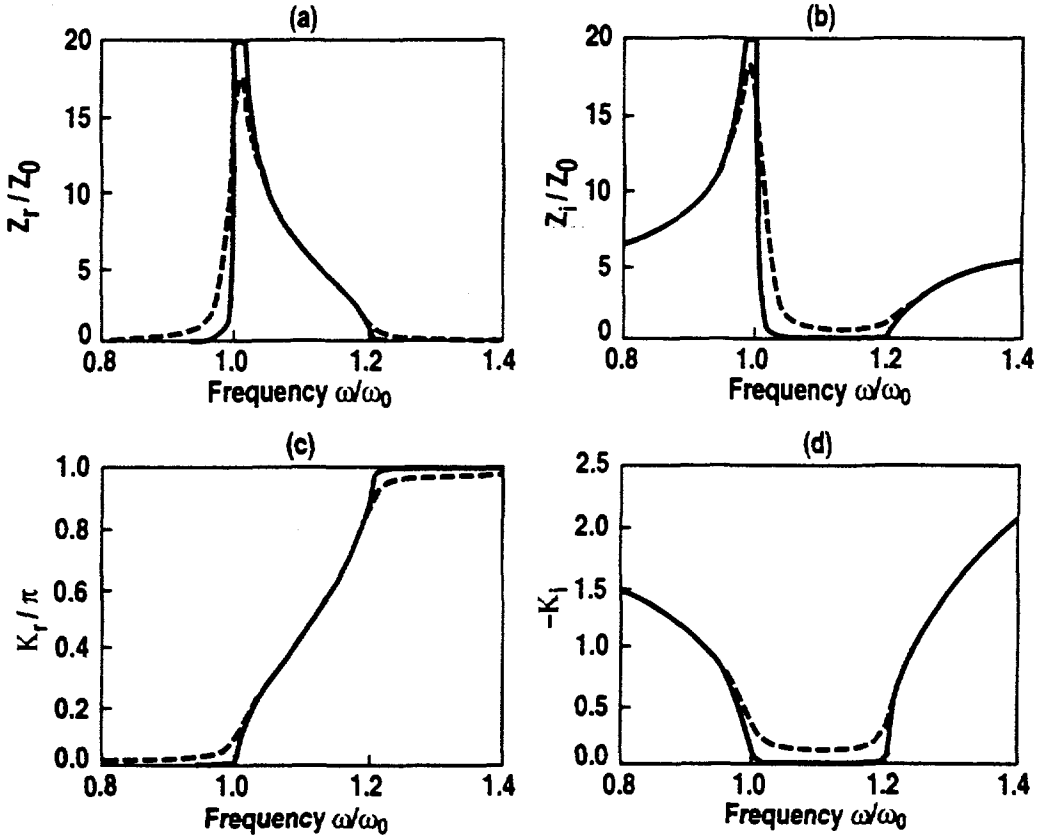

FIG. 3. Input impedance Z and real and imaginary part of the propagation constant K of the circuit shown in Fig. 2(a) as a function of frequency. Parameters are: $\omega_0 L_a/Z_0 = 0.1$, $\omega_0 L/Z_0 = 10$, dotted line $R_a/Z_0 = 0.02$, solid line $R_a/Z_0 = 0.002$.

dependence of K_r indicates that the strap-to-strap phase velocity is continuously frequency tunable. This is an important feature for the plasma current drive. Dependence of K_r on R_a is very weak as we see in Fig. 4(c), *i.e.*, the antenna loading does not change phasing.

II.B. Mutual Inductance-Coupled Resonator Circuit

With voltages across the capacitors and current in the LC resonators given in the form of Eq. (1), one finds the impedance and the wavenumber in the combline case shown in Fig. 2(c),

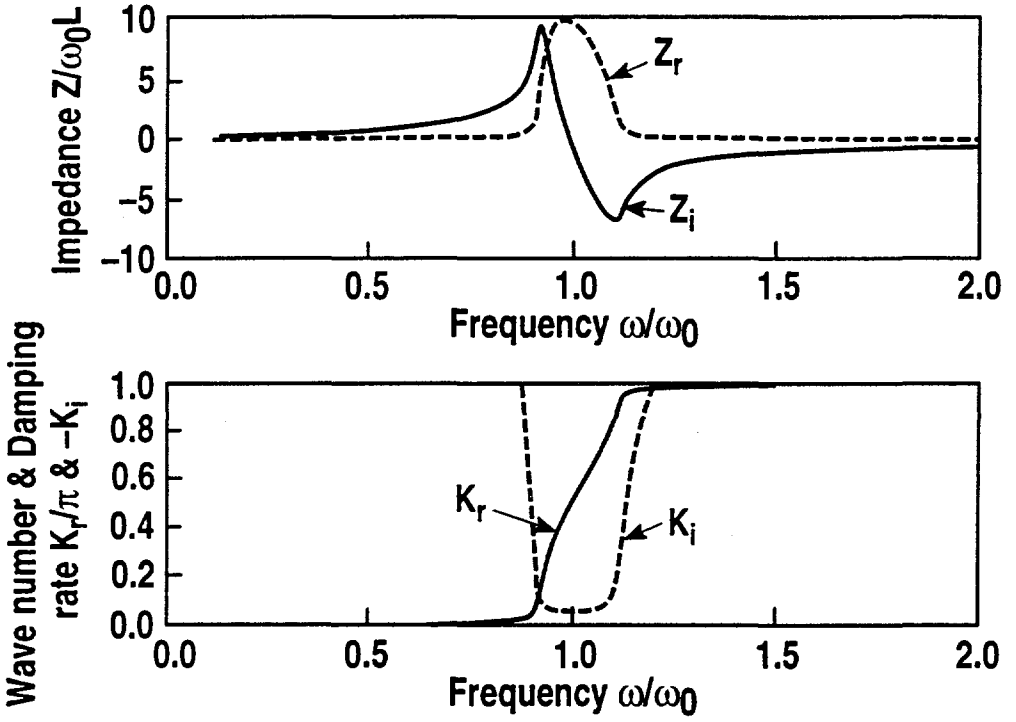

FIG. 4. Input impedance Z_c and the propagation constant K of the circuit shown in Fig. 2(c) as a function of frequency. Parameters are $M/L_c = 0.01$, $R/\omega_R L_c = 0.01$.

$$\left.\begin{aligned} Z_c &= \frac{i\omega L_c + R + i\omega M\, e^{iK}}{1 - \omega^2 L_c C + i\omega CR - \omega^2 MC\, e^{iK}} \\ e^{iK} &= -\frac{1}{2}\left(F + \sqrt{F^2 - 4}\right) \\ F &= \frac{1}{\omega^2 MC} + \frac{L_c}{M} + \frac{R}{i\omega M} \end{aligned}\right\} . \tag{4}$$

Here, R represents the sum of the strap ohmic resistance and the radiation resistance. The inductance L_c and the capacitance C are determined by the strap geometry and M is the mutual inductance between the straps. Each LC circuit resonates at $\omega_R = 1/(LC)^{1/2}$.

Both Z_c and K as functions of frequency are shown in Fig. 4. The frequency dependence of K is almost identical to the former case. The imaginary part K_i in the passband increases as R is increased and the real part K changes from nearly zero at the lowest end of the passband to π at the highest frequency end. The frequency dependence of the impedance is somewhat different. The real part Z_{cr} is highest at the midband instead of the lowest end and Z_{ci} swings from inductive to capacitive. In the Smith chart representation of impedance, however, the latter impedance characteristic is obtained (approximately) by tuning the former one by $\pi/2$. Thus, the frequency dependences of Z can be made similar to Z_c by adding a one-eighth wavelength transmission line of midband impedance to the former circuit.

The calculations for the finite length system are slightly more complicated than the above calculations and will be given later in this report, when needed to compare theory with the experimental results.

III. Experimental Setup

We have tested a traveling wave antenna in the DIII–D tokamak by using the existing four-element antenna with external coupling. A schematic diagram of the four-strap antenna and rf circuit is shown in Fig. 5. Each branch consists of a 30 Ω coaxial feedthrough which is terminated by two straps stacked poloidally in the tokamak and connected in parallel. Each branch forms a resonator. The resonance frequencies of four branches are adjusted to be equal within a difference of 100 kHz in the 50 to 90 MHz range by adding short coaxial cables at the opposite side of the straps. The nearest neighbor branch resonators are then coupled by adding the externally connected inductor coils in addition to inherent mutual inductances between the straps. This creates a four-element slow wave structure. By changing the external inductors, the transmission bandwidth may be controlled. Without the external inductors, the mutual inductance between the straps gives a bandwidth of only 3% of the center frequency. The bandwidth is increased up to 20 MHz (*i.e.*, 30%) by adding the external inductors. The matching adjustments to the external 50 Ω cables are made by adjusting the tapping points at both input and output sides (see Fig. 5).

Low signal power, 100 W, is fed by a 50 Ω cable to one end of the antenna circuit. The other end is termined in 50 Ω. A directional coupler is inserted at the input side to pick up both forward and reflected signals and at the output side to pick up the transmitted signal. Using a network analyzer connected to the DIII–D digital data system, these signals are corrected to complex reflection and transmission coefficients as a function of the selected frequency or frequency band for each plasma shot.

The DIII–D tokamak[10] has capabilities of controlling the plasma shapes and positions which are useful for changing the antenna loading. The measurements of antenna characteristics were carried out with H– and VH–mode plasmas which exhibit discharge mode transitions, ELM activities, and disruptions. The parameter ranges employed are: the toroidal field B_t = 1 to 2 T, the toroidal current I_p = 0.5 to 1.5 MA, the electron temperature T_e = 0.5 to 4 keV, and the plasma density = (0.05 to 1) × 10^{20} m^{-3}. The working gas was deuterium.

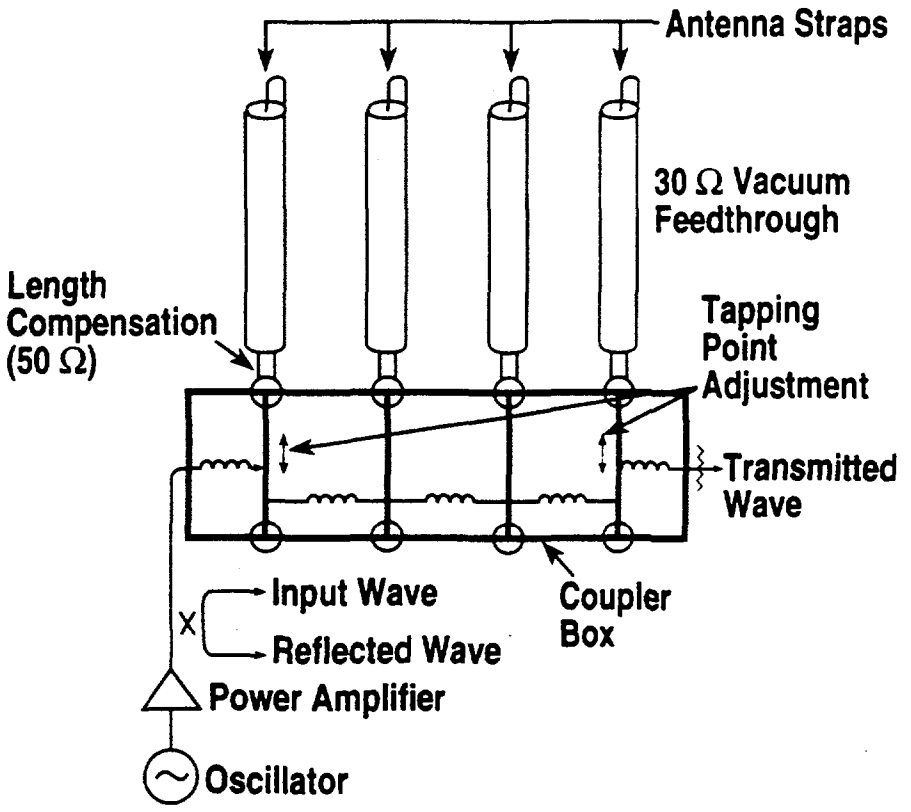

FIG. 5. Schematic diagram of the traveling wave antenna arrangement on the DIII–D tokamak.

IV. Experimental Results

We first give an example of small signal transmission through the traveling wave structure, the reflection from the input, and the input-output phase difference as a function of frequency with and without the presence of plasma. In the case shown in Fig. 6, the external coupling inductors are added and the impedance is matched to the external 50 Ω system at the middle of the transmission band by adjusting the tapping points when there is no plasma. Both transmission and reflection curves show the band-pass characteristic. The input-output phase delay (chosen to be in the negative direction) is small at the lower frequency end of the passband and increases to about 3.5π at the high frequency end. Since we have four-strap antenna, this result is consistent with the calculations as shown in Fig. 3. Note that the phase delay increases up to slightly less than π/strap.

The data are taken during periods when the tokamak is operated for many plasma shots without changing the discharge parameters, *i.e.*, similar plasmas are reproduced many times. This enables us to confirm repeatability and to present a complete set of data. The data set in Fig. 6 shows that the transmission decreases by 3 to 6 dB in the presence of plasma. The data show that the decrement is larger at the low frequency where the toroidal wavelength is longer. This frequency dependence is interpreted in the next section.

In order to test the insensitivity of the reflected power to plasma loading, the measurements were carried out in discharges having ELMs, which introduce a large change in the density profile at the plasma boundary and antenna loading. The D_α signal in the divertor indicates that ELMs occur during the neutral beam injection. The electron density measured by the Thomson scattering system at three radial positions (3.5 cm apart) near the plasma boundary indicates that the L– to H–mode transition occurs at 1600 msec. The start of ELMs reduces the outermost density significantly. The magnetically determined plasma-wall gap changes 4 to 8 cm during the plasma shot. The plasma current disrupts at 5100 msec. The reflected power from the antenna system at 51.4 and 52.4 MHz shown at the bottom of Fig. 7 show very little change throughout all these plasma activities.

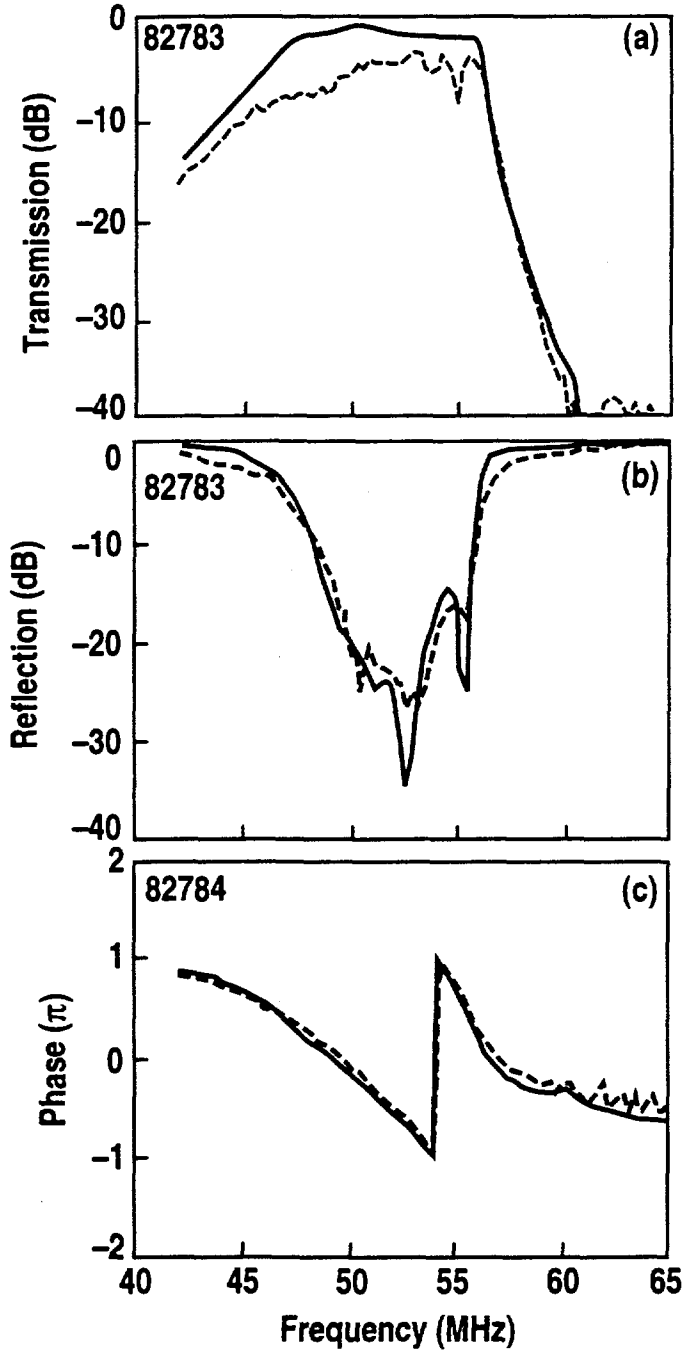

FIG. 6. Transmission through the traveling wave antenna (a), reflection from the input (b), and the input-output phase delay as a function of frequency (c). Curves both with and without plasma loading are shown. The numbers in the upper left corners are the discharge shot numbers of the DIII–D tokamak. For the discharge with plasma, the toroidal field is 2 T, the density is 6×10^{13} cm^{-3}, and the plasma curent is 0.7 MA. The field configuration is single null divertor, and the plasma-antenna gap is 5 cm.

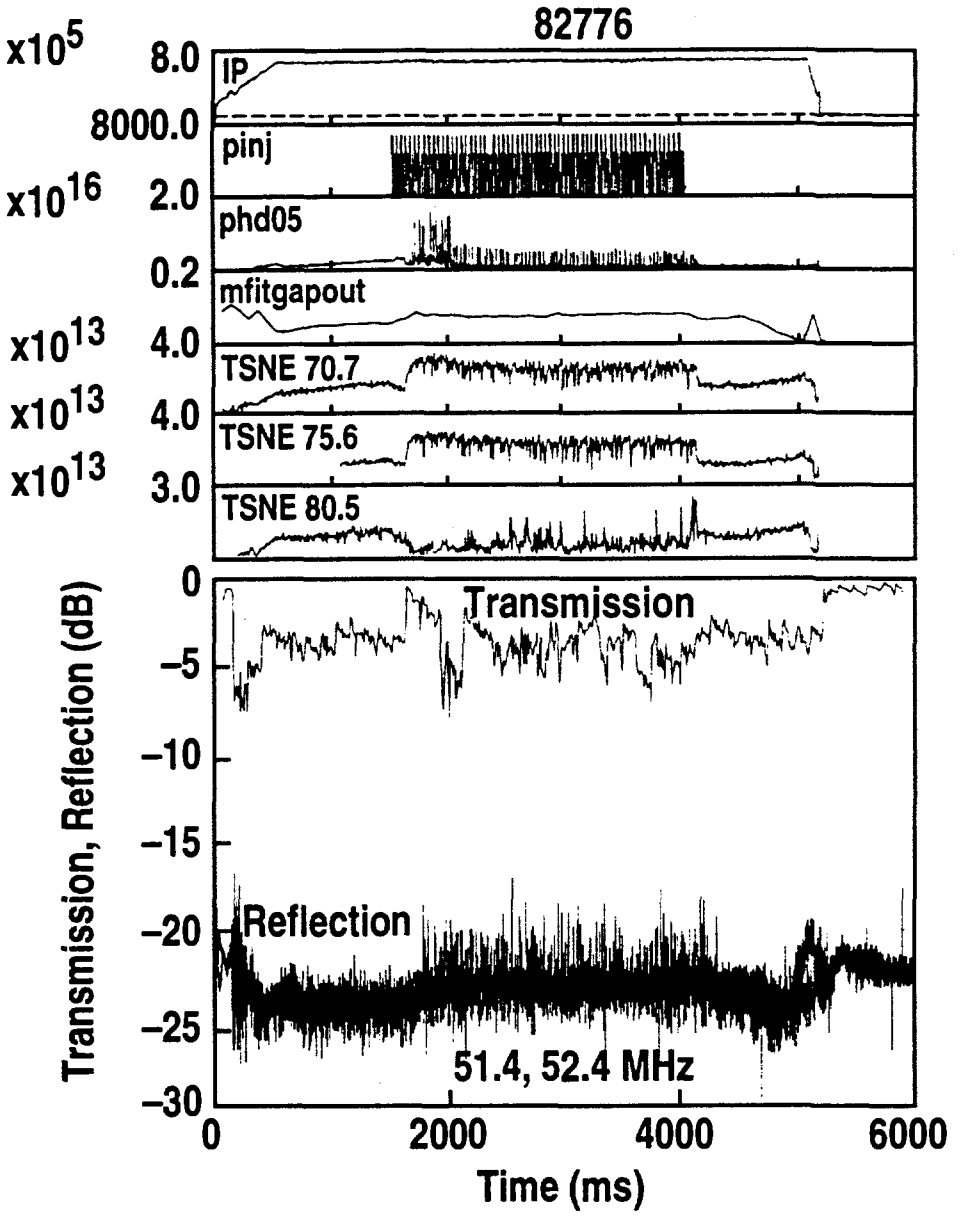

FIG. 7. (a) Some plasma parameter signals of the tokamak plasma when the measurements on antenna are carried out. "IP" is the plasma current, "TSNE" is the electron density measured by the Thomson scattering at the indicated position in centimeters, "beams" is the injected neutral beam power, "phd05" is the D_α emission from the divertor, and "mfitgapout" is the magnetically determined wall-plasma boundary gap in meters. Spikes of the phd05 signal indicate ELMs. (b) Time dependence of (reflected power)/(incident power) at 51.4, 52.4, and 55.4 MHz and (transmitted power)/(incident power) in the 51.4 to 55.4 MHz band (dots).

The Smith chart representation of the input impedance during the whole period of the plasma discharge with ELMs is shown in Fig. 8. The black overlay located near the center of the Smith chart represents the impedance measured at three different frequencies (51.4, 52.4, and 54.4 MHz) throughout three similar plasma shots. Note that the impedance stays within a small area near the center (where the matching is perfect) indicating that good impedance matching is maintained. A circle around the impedance data indicates that the reflected power is 3% (VSWR = 1.4). Within this circle, the rf transmitter is operated without problem. The transmission shown in Fig. 7(b) represents the data obtained in a frequency band covering the above three frequencies on a similar plasma shot. The loss radiation (*i.e.*, power coupled to the plasma) stays in a range of −3 to −5 dB most of the time but reaches −6 to −8 dB at the start of the giant ELMs.

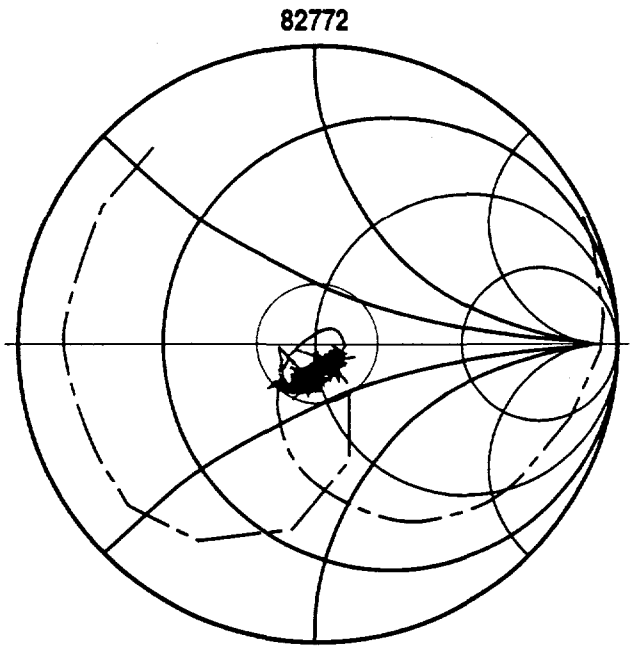

FIG. 8. Smith chart representation of input impedance at 51.4, 52.4, and 54.4 MHz. The fuzzy dot shows the impedance during the whole plasma discharge. The smooth (curly) curve is obtained by sweeping the frequency in vacuum. A small circle indicates VSWR = 1.4.

These measurements were repeated for a traveling wave antenna with a wider passband of bandwidth/center frequency $\equiv \Delta\omega/\omega = 32\%$. This was achieved by reducing the external coupling inductance. The impedance matching was maintained by repositioning the tap point. The plasma contributes very little effect, *i.e.*, the decrement of transmission and the change of reflection by the plasma loading is much smaller compared to the former narrower band case ($\Delta\omega/\omega = 20\%$).

To test the other extreme of narrow bandwidth, the external inductors were eliminated so that the passband width is totally determined by the mutual inductance between the antenna straps. The data shown in Fig. 9 represents the higher passband of the traveling wave antenna arising at the higher frequency where the resonance length of each resonator is three-quarters of a wavelength. The plasma loading reduces the transmission by about 20 dB and the passband shifts upward. The reflection coefficient also changes significantly in level and frequency upshift. Note for example that the pronounced reflection dip at 93.3 MHz, which is made by the tapping point adjustment, is totally eliminated by the plasma loading. This behavior is common to all plasma modes suggesting that such narrow bandwidth is not useful for actual high power use.

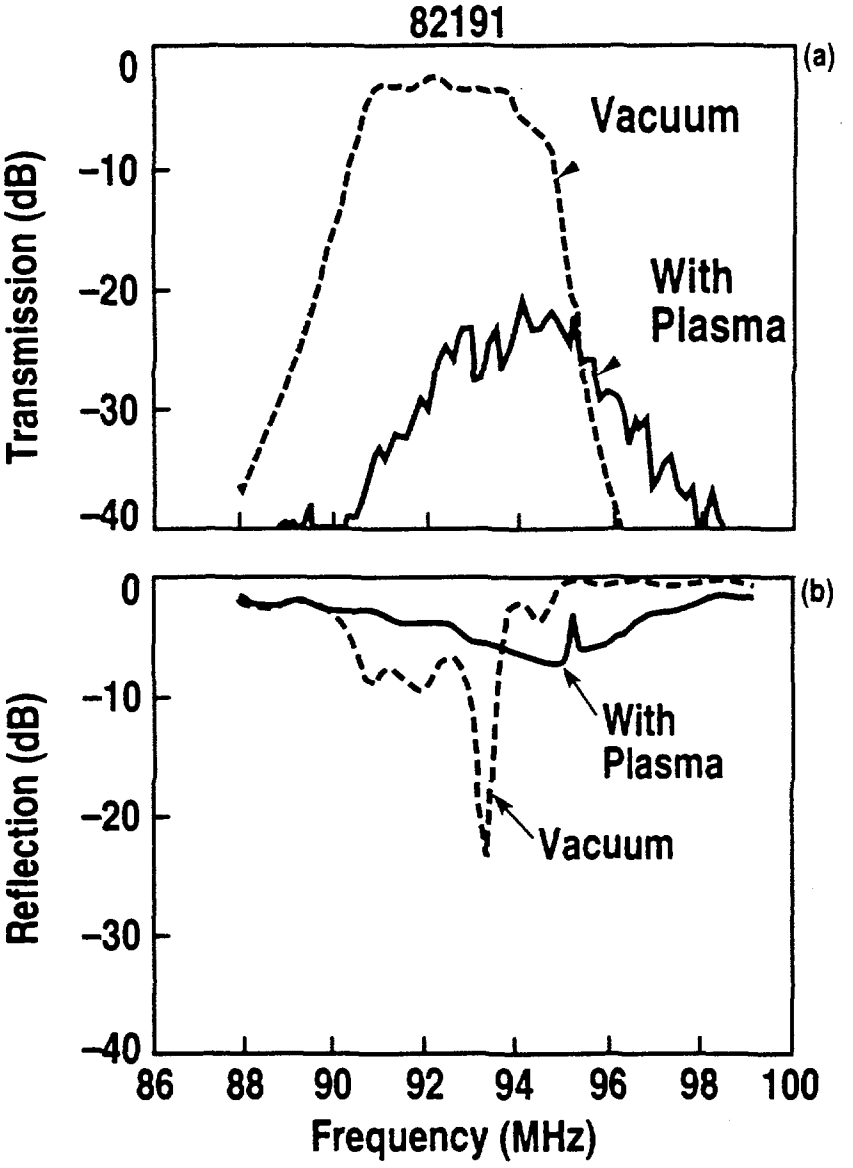

FIG. 9. Transmission and reflection as a function of frequency when antenna elements are coupled only through the mutual inductance between the antenna straps. Data with and without plasma are shown. The bumps at 95 MHz are markers.

V. Comparison Between Experiments and Model

Let us consider a four-element system instead of the half-infinite system discussed in Section II. The voltage and the current at the midpoint of the n-th coupling inductor is given by the sum of positive and negative going waves,

$$\left.\begin{aligned} V(n) &= V_+ \exp(i\omega t - iKn) + V_- \exp(i\omega t + iKn) \\ ZI(n) &= V_+ \exp(i\omega t - iKn) - V_- \exp(i\omega t + iKn) \end{aligned}\right\} , \tag{5}$$

where Z is given by Eq. (2). The external circuit of impedance Z_{ext} is attached on both input and output ends of the antenna system. The boundary condition at $n = 4$, that both voltage and current are continuous, determines V_+/V_- as a function of Z/Z_{ext}. The input impedance of a four-element system is found to be

$$Z_4 = Z\,\frac{(1 + Z/Z_{\text{ext}}) + (1 - Z/Z_{\text{ext}})\,e^{-i8K}}{(1 + Z/Z_{\text{ext}}) - (1 - Z/Z_{\text{ext}})\,e^{-i8K}} \quad . \tag{6}$$

The ratios reflected to incident wave voltage and transmitted to incident wave voltage are given by

$$\left.\begin{aligned} V_{\text{r}}/V_{\text{i}} &= (Z_4/Z_{\text{ext}} - 1) \;/\; (Z_4/Z_{\text{ext}} + 1) \\ V_{\text{t}}/V_{\text{i}} &\equiv V(4)/V_{\text{i}} \\ &= \left[\cos 4K + \frac{1}{2}\, i\,(Z_4/Z_{\text{ext}} + Z_{\text{ext}}/Z_4)\, \sin 4K\right]^{-1} \end{aligned}\right\} . \tag{7}$$

The normalized reflected and transmitted powers are $|V_{\text{r}}/V_{\text{i}}|^2$ and $|V_{\text{t}}/V_{\text{i}}|^2$.

It is noted here that changing tap points as we have done experimentally is equivalent to inserting variable step-up ratio transformers between the antenna system and the external circuit. Thus changing Z_{ext} is the same as changing the tap point. Another important point which should be made here is that good impedance matching must be made at both ends of the traveling wave structure in order to have wave directivity. The reflection from the output end creates a negative going wave V_- which deteriorates the directivity.

Since the wave magnetic field in the vacuum gap between the antenna and the plasma boundary decays like $\exp(-gK_r/S)$, the antenna resistance which is proportional to the wave power is modeled by

$$R_a = R_R \exp(-2gK_r/S) + R_0 \quad . \tag{8}$$

Here, g is the gap distance, S is the separation between the adjacent antenna straps, and R_0 is the ohmic resistance of the antenna. We choose the radiation resistance R_R as a parameter to be determined by fitting the experimental results.

The results of an example computation using the above analytical model are exhibited in Fig. 10. These are the reflection and transmission spectra that fit the observations given in Fig. 6. We choose R_0 to fit the corresponding vacuum loaded data in Fig. 6. We then choose R_p to fit the plasma loaded data. Note that the modeled K_r dependence of the plasma loading causes the theoretical and measured profiles to be in remarkably good agreement. The good fit within the passband plateau indicates that this model can be a useful system design guideline.

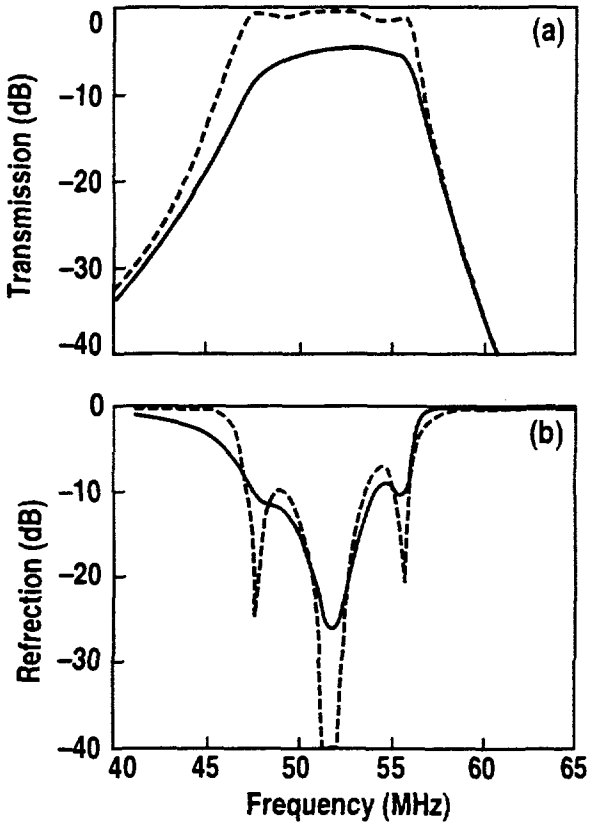

FIG. 10. Computed transmission, reflection, and Smith chart representation of the input impedance. Curves for both with and without loading are shown. Parameters are $R_0/Z_0 = 0.004$, $R_R/Z_0 = 0.07$, $\omega_0 L_a/Z_0 = 0.6$, $\omega_0 L/Z_0 = 11$, $Z_{ext}/Z_0 = 5$,g=9 cm, $\omega_0/2\pi = 62$ MHz.

VI. Design Considerations

One purpose of the traveling wave antenna system is to avoid the need for dynamic tuning as plasma conditions change. A key parameter is the bandwidth which keeps the reflection below an allowable level for a given range of antenna resistance R_a. If the system is tuned to the external circuit when there is no plasma, the reflected power coefficient in the presence of plasma is given by

$$\mathcal{R}_p = \left| \frac{1 - Z(R_a)/Z(R_a = 0)}{1 + Z(R_a)/Z(R_a = 0)} \right|^2 \quad . \tag{9}$$

The value of $\mathcal{R}_p$ at the passband center frequency is estimated by using the half-infinite system model of Section II.A and plotted as a function of R_a/Z_0 in Fig. 11(a) for a few values of $\Delta\omega/\omega$, the bandwidth-to-center frequency ratio. The reflected power decreases as $\Delta\omega/\omega$ increases. The value of R_a/Z_0 in the experiments shown in Figs. 6 and 9 are in a range from 0.02 to 0.03. The curves for $\mathcal{R}_p$ at $\Delta\omega/\omega = 20\%$ and 3% indicate $-$(25 to 20) and $-$(10 to 6) dB, respectively, which are consistent with the observed values. If the tuning is made with the plasma loading instead of vacuum, smaller reflections are obtained over a larger range of R_a/Z_0.

The damping rate, *i.e.*, attenuation/strap, determines the number of straps necessary for radiating the majority of input power before the wave reaches the other end of the structure. From the plot shown in Fig. 11(b), which is computed for the half-infinite system), one finds 90% or more of the power is radiated within ten straps, *i.e.*, 1 dB/strap or more when $\Delta\omega/\omega = 20\%$ and $R/Z_0 > 0.02$. The narrower bandwidth is better for reducing the number of straps, but it creates larger reflection and larger damping spoils the wave spectrum so that the current drive capability is deteriorated. The computations to be presented in the next section indicate that the damping rate should be kept below about 2.5 dB/strap.

A candidate system having ten antenna elements satisfies the requirements discussed here, with some margin of safety. However, most tokamak antennas today do not have more than four elements. The recirculation of power, as discussed in the next section, allows us to use as-built antennas as traveling wave antennas.

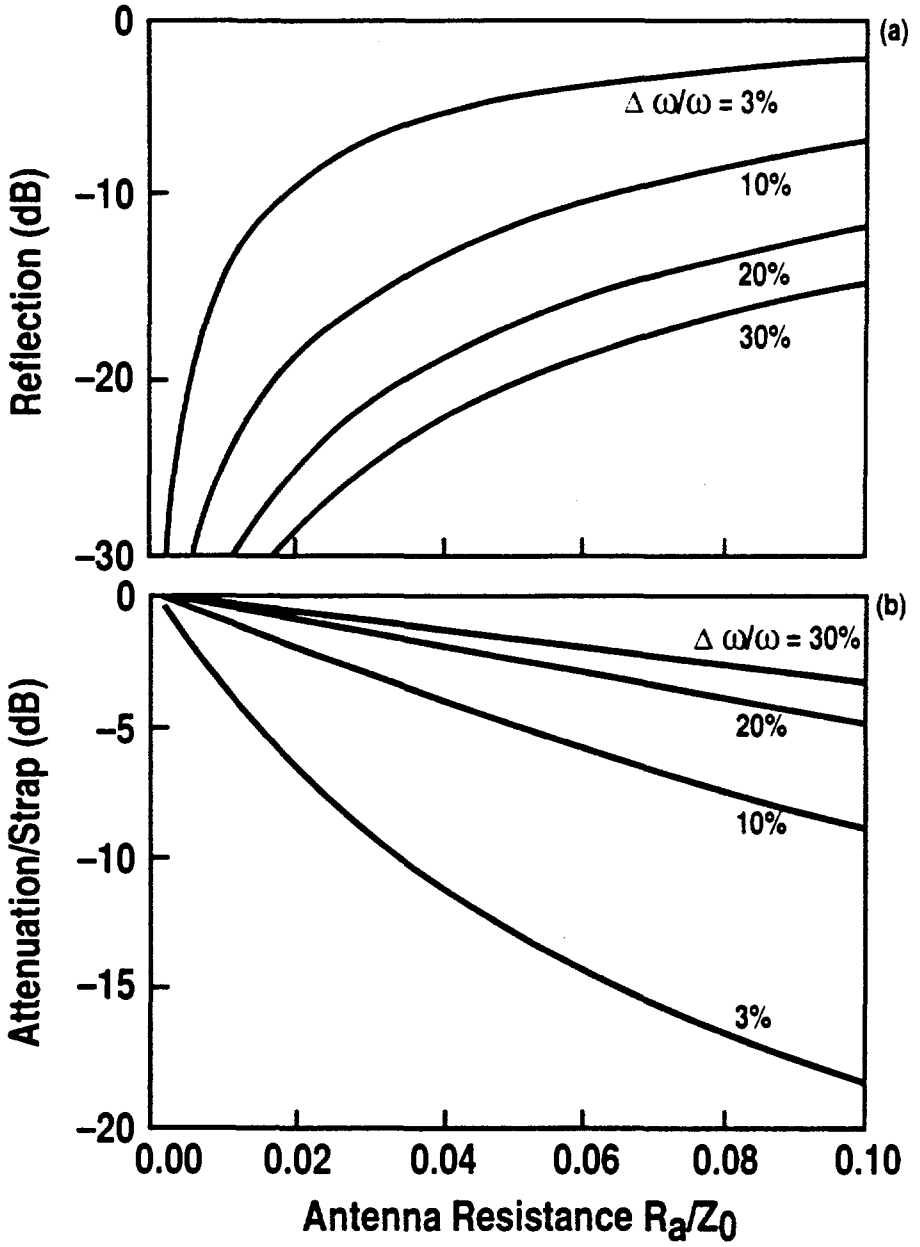

FIG. 11. Computed reflection and attenuation as a function of the antenna resistance. The frequency is at the center of the passband. A few values of (bandwidth)/(center frequency) = $\Delta\omega/\omega$ are taken.

VII. Recirculation Circuit

The recirculation circuit[11] increases the fraction of radiated power with fewer antenna elements. The experimental data shown in Fig. 7, for instance, indicate that only about one-half of the power fed into the antenna system is radiated during a single passthrough of the traveling wave structure. By recirculating the transmitted power back into the antenna system, more power can be radiated. This must be done without sacrificing the insensitivity of the plasma loading and the wave directivity to plasma conditions. The single pass power attenuation should be about 30% to 90%. Less than 30% means that over three times the input power is recirculating and the circuit resonance is too narrow. Over 90% means the circuit is not needed. We consider an example which is designed for the high power operations at DIII–D. The four-element traveling wave antenna consists of resonators shown in Fig. 2(b). The impedance of this system may be kept nearly equal to the external circuit impedance Z_{ext}, which is nearly equal to Z_0 ($Z_0 = 30\ \Omega$ and $Z_{\text{ext}} = 25\ \Omega$ in the DIII–D rf system). The recirculation circuit is shown in Fig. 12. The impedance matching sections, which consists of line stretcher and stub, are inserted on both input and output ends of antenna system.

The transmitter power is first fed into a directional coupler. A part of the power is fed to the antenna system and the rest goes to the dummy load. The power that passes through the antenna comes back to the directional coupler through the phase shifter. One finds immediately that all power from the transmitter may be radiated by adjusting the phase shifter if the directional coupler's coupling constant equals the attenuation in the antenna system. The purpose of the following discussions is to find if high radiation efficiency can be obtained for a wide range of plasma loading without dynamic tuning.

The characteristic of the directional coupler is given by

$$\begin{pmatrix} V_1 \\ V_2 \\ V_3 \\ V_4 \end{pmatrix} = \begin{pmatrix} 0 & b & ia & 0 \\ b & 0 & 0 & ia \\ ia & 0 & 0 & b \\ 0 & ia & b & 0 \end{pmatrix} \begin{pmatrix} v_1 \\ v_2 \\ v_3 \\ v_4 \end{pmatrix} , \tag{10}$$

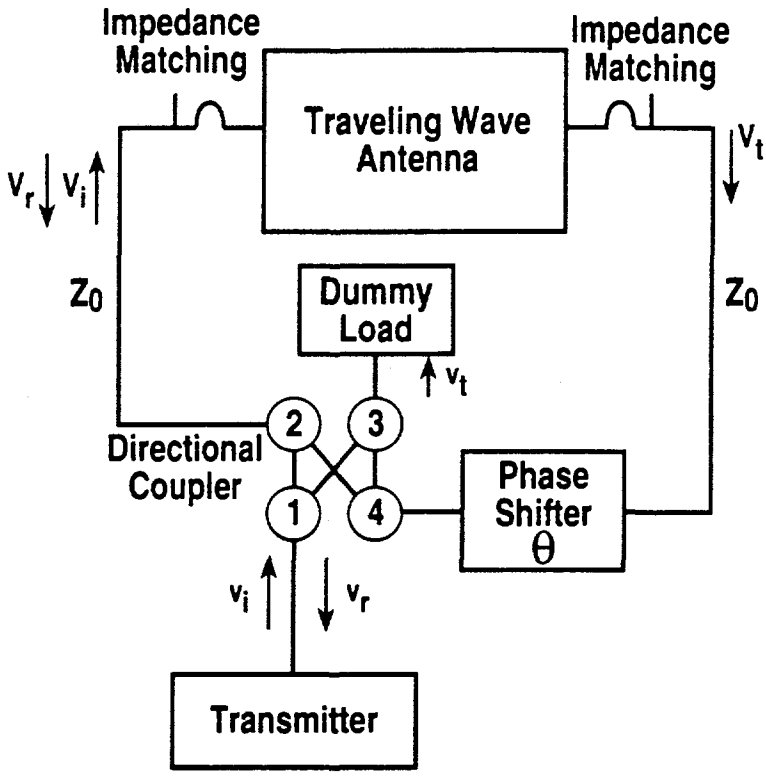

FIG. 12. A schematic diagram of power recirculation.

where V_j and v_j are the outgoing and incoming wave voltages to the port number j, and a and b are the coupling constants restricted by $0 \leqslant a \leqslant 1$ and $a^2 + b^2 = 1$. In the 3 dB coupler, for instance, they are $a = b = 1/2^{1/2}$. From simple wave circulation equations for the circuit, one easily finds the wave voltages going to the dummy load v_t and coming back to the transmitter v_r,

$$\left.\begin{aligned} \frac{v_t}{v_i} &= \frac{i}{a}\left[1 - \frac{1-a^2}{1 - ia\,e^{i\theta}\left(T + \dfrac{ia\,e^{i\theta}R^2}{1 - ai\,e^{i\theta}T}\right)}\right] \\ \frac{v_r}{v_i} &= \frac{(1-a^2)\,R}{(1+ia\,e^{i\theta}T)\left[1 - ia\,e^{i\theta}\left(T + \dfrac{ia\,e^{i\theta}R^2}{1 - ia\,e^{i\theta}T}\right)\right]} \end{aligned}\right\}, \qquad (11)$$

where

$$R = V_r/V_i \quad \text{and} \quad T = V_t/V_i \quad . \tag{12}$$

V_i, V_r, and V_t are the incident, reflected, and transmitted wave voltages to the antenna system, including the matching sections, v_i is the voltage of the incoming wave to the directional coupler from the transmitter, and θ is the phase delay in the phase shifter (see Fig. 12 for these notations).

The fraction of powers going to the dummy load $P_{trans}/P_i = |v_t/v_i|^2$, reflected back to the transmitter $P_{ref}/P_i = |v_r/v_i|^2$ and radiated into the plasma $P_{rad}/P_i = 1 - P_{trans}/P_i - P_{ref}/P_i$ are calculated as a function of antenna resistance R_a. The ohmic loss is neglected. A few examples obtained from different directional coupler constants are shown in Fig. 13. These curves are obtained by the parameter optimization which is the tuning process of the system.

We first choose the desired operation frequency in the passband and determine the matching section parameters by employing the no plasma loaded value of Z obtained from the half-infinitely long system. The reflected power is then minimized. P_{ref}/P_i can be suppressed below a few percent across the antenna system including the matching sections. The phase delay at the phase shifter is then determined in a way that the waves at the ports 1 and 4 of the directional coupler are added in port 2. This phase adjustment maximizes the radiated power.

The weaker coupling (smaller a) in the directional coupler shifts the maximum of the radiated power toward larger values of R_a which introduces larger single pass radiation attenuation. The radiated fraction remains large (say more than 90%) in a wider range of R_a when the coupling is weak, $a = 1/2$ (-6 dB) for example as shown in Fig. 13(a). In contrast, if the coupling is strong or a 6 dB coupler is employed and ports 2 and 3 are reversed, the majority of the power is damped in the dummy load when R_a is large [Fig. 13(c)]. Although the power reflected back to the transmitter may be kept small, this setup works only when the single pass attenuation is very weak. The recirculation is unnecessary if the single pass damping exceeds 10 dB, *i.e.*, more than 90% is radiated.

The following computations are carried out in order to find the attenuation constant above which the radiation spectrum is spoiled. We have computed the power spectrum

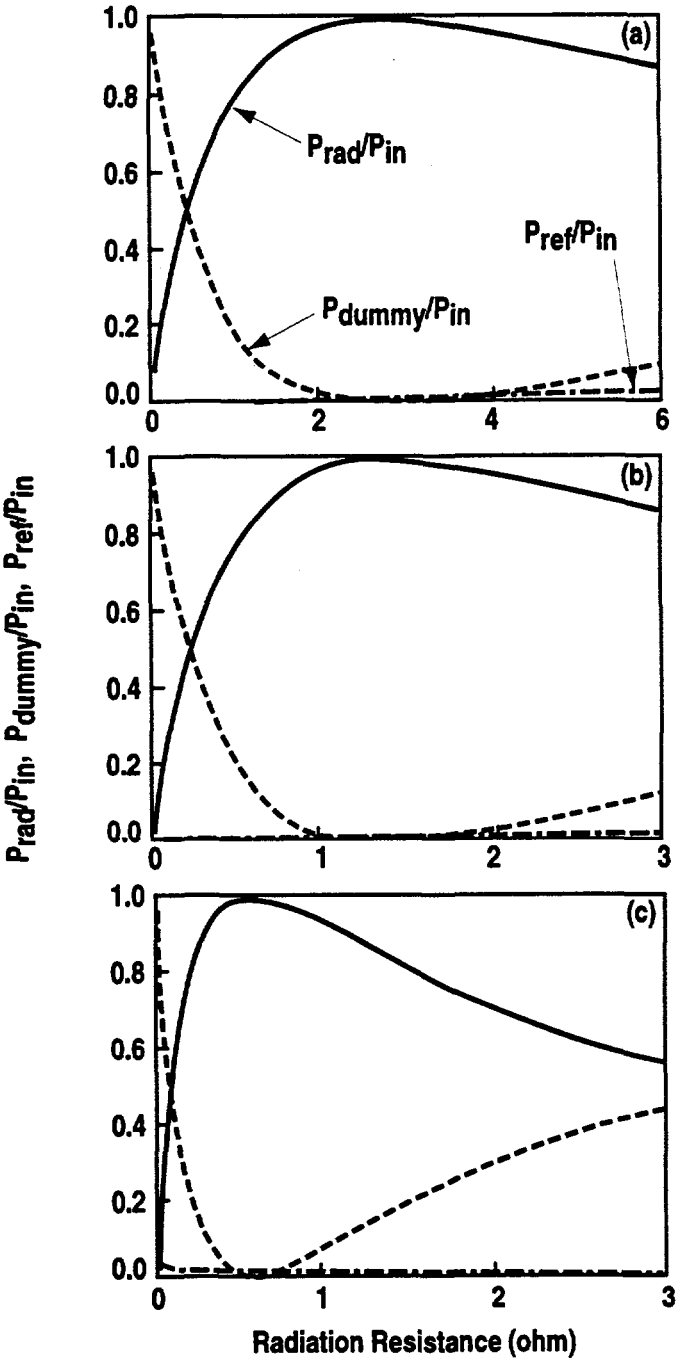

FIG. 13. Fraction of radiated power $P_{\rm rad}/P_{\rm in}$, dumped power into dummy load $P_{\rm trans}/P_{\rm in}$, and reflected power back to transmitter $P_{\rm ref}/P_{\rm in}$, as a function of antenna resistance when the power is recirculated. The directional coupler constants are (a) 6 dB, (b) 3 dB, and (c) 1.25 dB. Other parameters are $L = 100$ nH, $L_{\rm a} = 50$ nH, $\omega/2\pi = 90$ MHz, $\ell = 0.98$ m, $\ell' = 0.5$ m, $Z_0 = 30\ \Omega$, $Z_{\rm ext} = 25\ \Omega$. See Fig. 2 for definition of ℓ and ℓ'.

$$p(k) = \left| \int_{-\infty}^{\infty} I(x)\, e^{-ikx}\, dx \right|^2 \quad , \tag{14}$$

of the field of the four-element antenna given by

$$\left.\begin{aligned} I(x) &= \sum_{m=0}^{3} e^{m(i\Theta-\delta)}\, h(x-m)\, sin^2(2\pi x) \\ \text{where} \qquad h(x) &= \begin{cases} 1 & \text{for} \quad |x| \leqslant 1/4 \\ 0 & \text{for} \quad |x| > 1/4 \end{cases} \end{aligned}\right\} \quad . \tag{15}$$

Θ and δ are the phase difference and the decay rate between adjacent antenna elements, respectively. Computer plots of $p(k)$ indicate that the power spectrum does not change much as long as the single pass damping, $-20\ \log(4\,\delta)$, is less than 10 dB. The higher single pass damping ($>$ 10 dB) increases the power in the uniform background without changing the spectral width of the main lobe. We conclude that the coupling constant of the directional coupler should be chosen in the range 3 to 6 dB. The bandwidth should then be determined in a way that the single pass damping stays in a range of 2 to 10 dB.

VIII. Conclusions

Modeling indicates that the traveling wave antenna maintains good impedance matching during L– to H–mode transitions, ELM, and plasma disruptions, and that phasing can be controlled through shifts of frequency. These characteristics were verified in low power experiments on DIII–D using a four-strap antenna with external coupling inductors. The desirable features of the traveling wave antenna can be obtained using a small number of antenna elements if the power is recirculated through a properly designed external circuit.

IX. Acknowledgments

The authors wish to thank C.P. Moeller, R.I. Pinsker, C.C. Petty, and J.S. deGrassie for their valuable comments during the development of this work.

This is a report of work sponsored by the U.S. Department of Energy under Contract No. DE-AC03-89ER51114.

X. References

1. T.H. STIX, *Waves in Plasmas*, American Institute of Physics, New York (1992), Ch. 17.

2. J. JACQUINOT, V.P. BHATNAGAR, C. GORMEZANO, and THE JET TEAM, "JET Recent Results on Wave Heating and Current Drive: Consequences for Future Devices," *Plasma Phys. and Contr. Fusion*, **35** (1993) A35.

3. F.W. BAITY, D.B. BATCHELOR, K.C. BILLS, C.H. FOGELMAN, E.F. JAEGER, J.L. PING, B.W. RIEMER, P.M. RYAN, D.C. STALLINGS, D.J. TAYLOR, and J.J. YUGO, "Design of Long-Pulse Fast Wave Current Drive Antennas for DIII–D," *Radiofrequency Power in Plasmas*, Proc. 10th Top. Conf. Boston, Massachusetts, April 1–3, 1993 (AIP Conf. Proc. 289), p. 343, American Institute of Physics.

4. R.H. GOULDING, D.J. HOFFMAN, P.M. RYAN, G. BOSIA, M. BURES, D. START, T. WADE, C.C. PETTY, and R.I. PINSKER, "Power Compensators for Phased Operation of Antenna Arrays on JET and DIII–D," *Radiofrequency Power in Plasmas*, Proc. 10th Top. Conf. Boston, Massachusetts, April 1–3, 1993 (AIP Conf. Proc. 289), p. 351, American Institute of Physics.

5. D.B. REMSEN, J.S. deGRASSIE, W.P. CARY, R.I. PINSKER, C.P. MOELLER, W. ARNOLD, S. MARTIN, and E. PIVIT, "Feedback Control Fast Hybrid Tuners," *Proc. 15th Symp. on Fusion Engineering*, Piscataway, Massachusetts, October 11–15, 1993, p. 1088, Institute of Electrical and Electronics Engineers.

6. F. DURODIÉ and M. VERVIER, "Design of an Automatic Matching Device for TEXTOR's ICRH System," *Proc. Europhys. Top. Conf. on RF Heating and Current Drive of Fusion Devices*, Brussels, Belgium, July 8–10, 1992, Vol. 16E, p. 81, European Physical Society.

7. C.P. MOELLER, R.W. GOULD, D.A. PHELPS, R.I. PINSKER, "Combline Antennas for Launching Traveling Fast Waves," *Radio Frequency Power in Plasmas*, Proc. 10th Top. Conf. Boston, Massachusetts, April 1–3, 1993 (AIP Conf. Proc. 289), p. 323, American Institute of Physics.

8. C.P. MOELLER, S.C. CHIU, D.A. PHELPS, "A Comb Line Structure for Launching Unidirectional Fast Waves," *Proc. Europhys. Top. Conf. on RF Heating and Current Drive of Fusion Devices*, Brussels, Belgium, Vol. 16E, p. 53, European Physical Society.

9. G.L. MATTHAEI, "Comb-Line Band-Pass Filters of Narrow or Moderate Bandwidth," *Microwave J.*, **August**, 92, 1963.

10. R.D. STAMBAUGH and DIII–D TEAM, "DIII–D Research Program Progress," *Plasma Physics and Controlled Nuclear Fusion Research*, Proc. 13th Int. Conference, Washington, D.C., October 1–6, 1990, Vol. 1, p. 69, International Atomic Energy Agency.

11. D.A. PHELPS, C.P. MOELLER, C.C. PETTY, and R.I. PINSKER, "Conversion of the Four-Strap Array in DIII–D to a Tunable Traveling Wave Antenna," *Radio Frequency Power in Plasmas*, Proc. 10th Top. Conf. Boston, Massachusetts, April 1–3, 1993 (AIP Conf. Proc. 289), p. 339, American Institute of Physics.